Contour Code: Robust and Efficient Multispectral Palmprint Encoding for Human Recognition

Zohaib Khan, Ajmal Mian and Yiqun Hu
School of Computer Science and Software Engineering
The University of Western Australia
{zohaib,ajmal,yiqun}@csse.uwa.edu.au

Abstract

We propose 'Contour Code', a novel representation and binary hash table encoding for multispectral palmprint recognition. We first present a reliable technique for the extraction of a region of interest (ROI) from palm images acquired with non-contact sensors. The Contour Code representation is then derived from the Nonsubsampled Contourlet Transform. A uniscale pyramidal filter is convolved with the ROI followed by the application of a directional filter bank. The dominant directional subband establishes the orientation at each pixel and the index corresponding to this subband is encoded in the Contour Code representation. Unlike existing representations which extract orientation features directly from the palm images, the Contour Code uses a two stage filtering to extract robust orientation features. The Contour Code is binarized into an efficient hash table structure that only requires indexing and summation operations for simultaneous one-to-many matching with an embedded score level fusion of multiple bands. We quantitatively evaluate the accuracy of the ROI extraction by comparison with a manually produced ground truth. Multispectral palmprint verification results on the PolyU and CASIA databases show that the Contour Code achieves an EER reduction upto 50%, compared to state-of-the-art methods.

1. Introduction

The human palm contains rich information which can be used to recognize individuals. This information mainly includes the principal lines, the wrinkles and the fine ridges. The ridge pattern can be captured using high resolution scanners and is generally used for offline identification in forensics. The principal lines and wrinkles can be acquired with low resolution sensors and are suitable for user authentication. In addition to the superficial features in a palm, there is presence of subsurface features *i.e*. the palm veins, visible under infrared light. While palm lines are comparatively thin, they are in dense presence over the palm. On the other hand, palm veins are thick, while their pattern may be quite sparse over the same region. Figure 1 shows palm images captured in three different bands. The availability of such complementary features (palm lines and veins) allows for increased discrimination between the individuals. Moreover, the subsurface features are also useful for liveness detection for the prevention of spoof attacks [1].

(a) *Lines* ($\lambda = 460$nm) (b) *Veins* ($\lambda = 940$nm) (c) *Both* ($\lambda = 630$nm)

Figure 1. Palmprint features in multiple bands

Using *Multispectral Imaging (MSI)*, it is possible to simultaneously capture images of an object in the visible spectrum and beyond. MSI has been extensively used in the fields of remote sensing, medical imaging and computer vision to analyze information in multiple bands of the electromagnetic spectrum. In the past decade, biometrics such as the face [2, 3], iris [4] and fingerprints [5] have been investigated using multispectral images for improved human recognition. Recently, there has been an increasing interest in multispectral palmprint recognition. Despite the potential of multispectral information to improve palmprint recognition, the computational complexity is a major challenge which can be addressed by an efficient representation and matching framework.

With the advancement in imaging technologies, multispectral images of the palm can be acquired using non-contact sensors such as digital cameras. Non-contact biometrics are user friendly and socially more acceptable [6]. A monochrome camera and illuminations in different bands can be used to capture multispectral images of the palm [7, 8]. A contact device restricts the hand movement by the introduction of pegs. However, it reduces the user acceptability due to hygiene related issues. On the other hand, a non-contact palm imaging system contains variations due to translation, rotation and scale between different images.

2. Related Work

Palmprint recognition approaches are mainly focused on line-like feature detection, subspace learning or texture based coding [9]. Line detection based approaches generally extract palm lines using edge detectors. Huang *et al*. proposed a palmprint verification technique based on principal lines [10]. The principal lines in a palm were extracted using a modified finite Radon transform and a binary edge map was used for representation. However, the recognition based solely on the use of palm lines is insufficient since two individuals can have highly similar palm lines making it difficult to discriminate between them [11]. Although line detection can effectively extract palm lines, it may not be equally useful for the extraction of palm veins due to their weak intensity profile and broad structure.

A subspace projection can capture the global characteristics of a palm. However, the finer local details are not well preserved. Wang *et al*. fused palmprint and palmvein images and proposed the *'Laplacianpalm'* representation [12]. Unlike the eigenpalm [13] or the fisherpalm [14] which mainly preserve the global features, the *'Laplacianpalm'* representation attempts to preserve the local characteristics as well, while projection onto a subspace. In another work, Xu *et al*. [15] represented multispectral palmprint images as quaternions and applied quaternion PCA to extract features. A nearest neighbor classifier was used for palmprint recognition using quaternion vectors. The quaternion model did not prove useful for representing multispectral images of the palm and demonstrated low recognition accuracy compared to the state-of-the-art techniques.

Texture based codes like the Competitive Code (CompCode) [16] and the Orthogonal Line Ordinal Feature (OLOF) [17] extract the orientation of lines and have shown state-of-the-art performance in palmprint recognition. Briefly, in a generic form of orientation coding, the response of a palm to a directional filter bank is computed so that each directional subband has line features that lie in a specific orientation. Then the dominant orientation index from the directional subbands is extracted at each point to form the orientation code. Orientation codes can be binarized for efficient storage and fast matching unlike other representations which require floating point data storage and computations.

CompCode employs a directional bank of Gabor filters to extract the orientation of palm lines and uses a binary representation for matching. Han *et al*. [8] used a three level *'Haar'* wavelet fusion strategy for multispectral palmprints. CompCode was used for feature representation and matching. However, the wavelet fusion of multispectral palms only proved promising for blurred source images. Moreover, the approach required parameter selection for the Gabor filter from a set of training multispectral images, which makes it dependent on the training data.

OLOF emphasizes the ordinal relationship of lines by using mutually orthogonal filter pairs to extract the feature orientation at a point. Hao *et al*. [18] used various pixel-level image fusion techniques and the OLOF representation for multispectral palmprint recognition. The feasibility of using multispectral images in a contact free environment was demonstrated to improve the recognition performance compared to the use of only monochrome images. The best recognition performance was achieved when the Curvelet transform was used for band fusion. Kisku *et al*. [19] proposed wavelet based band fusion and Gabor wavelet feature representation for multispectral images of the palm. Ant Colony Optimization (ACO) algorithm was applied to reduce the dimensionality by feature selection. Normalized Correlation and SVM were separately tested for classification. However, the wavelet based band fusion did not improve palmprint recognition performance compared to the Curvelet Fusion with OLOF [18].

Recently, Zhang *et al*. [1] analyzed palmprint matching on individual bands and showed that the Red band performs better than Near IR, Blue and Green bands. A score level fusion of individual bands revealed a superior performance compared to any single band. Guo *et al*. proposed the Binary Orientation Co-occurrence Vector (BOCV) [20] which encodes more than one orientation at the points of crossover lines in a palm based on a threshold computed from training palm images. The experiments showed that the BOCV is less sensitive to small rotation variations which is likely to be a consequence of multiple orientation assignments. However, a fixed threshold may lead to the detection of false multiple orientations at some points. A joint palmline and palmvein approach for multispectral palmprint recognition was proposed by Zhang *et al*. [11]. They designed separate feature extraction methodologies for palm line and palm vein and later used score level fusion for computing the final match. The approach yielded promising results, albeit at the cost of increased complexity.

Although, most of the existing palmprint representations may be extended to multispectral palmprints, they may not fully preserve the features that appear in different bands, *i.e*. both lines and veins. Moreover, existing research suggests that a score level fusion of multispectral bands is promising compared to a data level fusion using multi-resolution transforms. In this paper, we propose *Contour Code*, a novel orientation and binary hash table based encoding for robust and efficient multispectral palmprint recognition. The *Contour Code* representation is derived from the coefficients of the Nonsubsampled Contourlet Transform (NSCT) which has the advantage of robust directional frequency localization. Unlike existing orientation codes, which apply a directional filter bank directly to a palm image, we propose a two stage filtering approach to extract only the robust directional features. We select the combination that captures

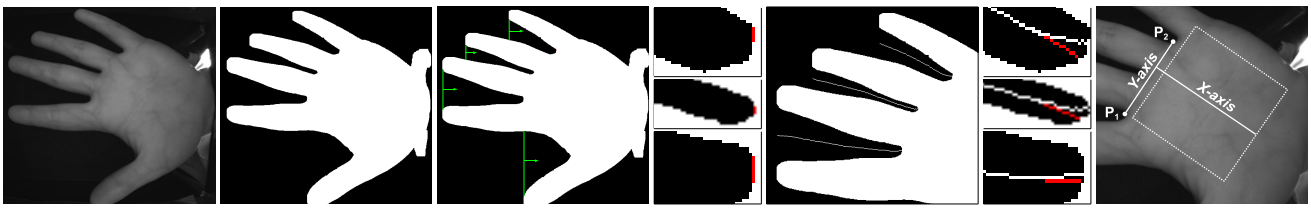

(a) (b) (c) (d) (e) (f) (g)

Figure 2. Extraction of ROI from a contact free hand image (a) Sample image (b) Preprocessed binary image (c) Start search for mid points (green) (d) Terminate search (red) (e) Located mid points (f) Extrapolation of mid points by polynomial fit (red) (g) ROI location

robust information in a multispectral palm for recognition. We develop a single methodology for the extraction of both the line and vein features. The *Contour Code* is binarized into an efficient hash table structure that only requires indexing and summation operations for simultaneous one-to-many matching with an embedded score level fusion of multiple bands.

3. Region of Interest Extraction

We used the PolyU (contact based) [21] and CASIA (contactless) [22] multispectral palmprint databases. Both contain low resolution (<150 *dpi*) multispectral images of palms stored as 8-bit monochrome images per band. The ROIs in the PolyU database were extracted according to the method in [23] and are available with the database. The images in the CASIA database contain high translation, scale and rotational variations. Here, the extraction of a reliable ROI is a challenge which is addressed in this paper. Detailed information of the databases is given in Table 1.

Database	**PolyU**	**CASIA**
Palms	500	200
Samples	12	6
Total MSIs	6000	1200
Bands	4	6
Central (nm) **Wavelength**	470, 525, 660, 880	460, 630, 700, 850 940, White

Table 1. Details of the PolyU and CASIA databases

In order to extract an ROI from the non-contact images, it is necessary to define some reference *landmarks* from within the image which describe the relative translation, scale and rotation between different image samples, repeatedly and accurately. Among the various features commonly used in hand geometry recognition, the valleys between the fingers are a suitable choice for the landmarks due to their invariance to the movement of a hand.

3.1. Preprocessing

The hand image in Fig. 2a is first thresholded to get a binary image. Smaller objects, not connected to the hand, that appear due to noise are removed using binary pixel connectivity. Morphological closing is carried out with a square structuring element to normalize the contour of the hand. Finally, any holes within the hand pixels are filled using binary hole filling. These operations are necessary for a successful landmarks localization. The resulting preprocessed binary image $B_{x,y}$ is shown in Fig. 2b.

3.2. Localization of Landmarks

Given $B_{x,y}$, in which the foreground pixels correspond to the hand, the localization proceeds as follows. In a column wise search (Fig. 2c), the binary discontinuities, *i.e.* the edges of the fingers are identified. From the edges, the gaps between fingers are located in each column and the mid points of all the gaps are computed. Continuing towards the valley of the fingers, the column encountered next to the last column should contain hand pixels (Fig. 2d). The search is terminated when fourth such closing of a valley is recorded. This column search assumes the hand rotation to be not more than $\pm 90^\circ$ in the image plane.

The mid points are then clustered corresponding to four finger valleys and the cluster corresponding to the index-thumb valley is discarded. Due to the natural contour of the fingers, it can be observed that the mid points do not follow a linear trend towards the valley as shown in Fig. 2e. Therefore, a second order polynomial is fitted to each valley's set of mid points excluding the last t points which tend to deviate from the path towards the landmark. The estimated polynomial is then used to approximate and extend the mid points in the last t points towards the valley as shown in Fig. 2f. We set t as 10% of the total number of mid points T of a valley. The final location of a landmark is the last encountered background pixel in the sequence of extrapolated points. The procedure is summarized in Algorithm 1.

3.3. ROI Extraction and Inter-band Registration

After the localization of landmarks, the ROI can be located for extraction. The landmarks P_1 and P_2 form a reference line segment, the *Y-axis*. Instead of selecting a bisector of the *Y-axis* for determination of the *X-axis*, we fix *X-axis* at two-thirds of the distance from P_1 to P_2 to centralize the ROI over the palm (see Fig. 2g). The average palm width serves as the scale identifier to extract a scale invariant ROI. In our experiments, the ROI side length is scaled to 70% of

Algorithm 1 Localization of Landmarks

Require: $B_{x,y}, i \leftarrow 0, c \leftarrow 1$
Ensure: P_1, P_2, P_3
  while $i < 4$ **do**
    $n\_gaps \leftarrow$ number of gaps in column $B_{c,y}$
    for $g = 1$ to n_gaps **do**
      $\mathbf{P}^M_{x,y} \leftarrow mid(g)$
      if End of Gap **then**
        $i \leftarrow i + 1$
      end if
    end for
    $c \leftarrow c + 1$
  end while
  Divide $\mathbf{P}^M_{x,y}$ into 4 clusters
  for $j = 1$ to 3 **do**
    Fit Polynomial ξ_j to $(T_j - t_j)$ points of $\mathbf{P}^{jM}_{x,y}$
    Extrapolate t_j points using ξ_j
    $P_j \leftarrow$ coordinates of last background pixel
  end for

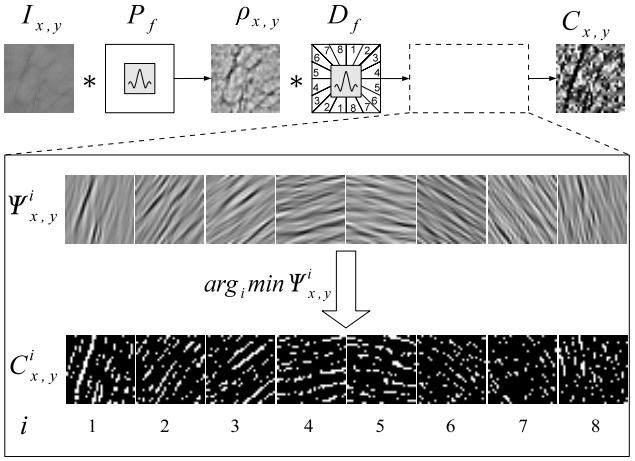

Figure 3. Extraction of the *Contour Code* representation of $I_{x,y}$. $\rho_{x,y}$ is the pyramidal bandpass subband. $\Psi^i_{x,y}$ are the bandpass directional subbands. The images $C^i_{x,y}$ represent the dominant points existing in the i^{th} directional subband. The intensities in $C_{x,y}$ correspond to $i = 1, 2, ...8$ (from dark to bright).

the palmwidth. The distance of the center of ROI on *X-axis* is also made proportional to the scale. Knowing the angle of rotation of the hand, θ the ROI can be directly extracted from the input image using an affine transformation. The same region is extracted from the remaining bands of multispectral palm image.

As there is a possibility of minor movement of a hand during acquisition of a multispectral image, a sequential band registration of ROIs is carried out. *Band 2* is registered to *Band 1* then *Band 3* is registered to the registered part of *Band 2* and so on. Since, there is negligible rotation and scale variation within the consecutive bands, we limit the registration search space to ± 2 pixel translation in both dimensions. The registered ROIs are then down-sampled to 32×32 pixels using bicubic interpolation. This resampling step has several advantages. First, it suppresses the inconsistent lines and noisy regions. Second, it reduces the storage requirement for the final *Contour Code*. Third, it largely reduces the time required for the extraction of features and matching.

4. Contour Code

4.1. Multidirectional Feature Encoding

We utilize the nonsubsampled contourlet transform (NSCT) [24], a multi-directional expansion having improved directional frequency localization and efficient implementation compared to its parent, the contourlet transform [25]. The NSCT has been effective in basic image processing applications such as image denoising and image enhancement. In this work, we exploit the directional frequency localization characteristics of the NSCT for orientation feature extraction in palmprint images.

An ROI $(I_{x,y})$ of size $m \times n$ is first convolved with a nonsubsampled bandpass pyramidal filter (P_f) which captures the details in the palm at a single scale as shown in Fig. 3. This filtering operation allows only the robust information in a palm to be passed on to the subsequent directional decomposition stage. The band pass filtered image $(\rho_{x,y})$ is subsequently subjected to a nonsubsampled directional filter bank (D_f), comprising 2^k directional filters. We selected a third order directional filter bank ($k = 3$) resulting in 8 directional subbands $(\Psi_{x,y})$. Therefore, each directional subband covers an angular region of $180/8 = 22.5°$. The choice of filters for the pyramidal and directional decomposition stages is determined by their line feature capturing ability. We perform a detailed experiment for the selection of pyramidal-directional filters in Section 5.2.

Generally, both the line and vein patterns appear as dark intensities in a palm and therefore correspond to a negative filter response. The orientation of a feature is determined by the coefficient corresponding to the minimum peak response among all directional subbands at a specific point. Let $\Psi^i_{x,y}$ denote the coefficient at point (x, y) in the i^{th} directional subband where $i = 1, 2, 3, ..., 2^k$. We define a rule similar to the competitive rule in [16] to encode the dominant orientation at each (x, y).

$$C_{x,y} = \arg\min_i \Psi^i_{x,y} \tag{1}$$

where $C_{x,y}$ is the *Contour Code* representation of $I_{x,y}$. Similarly, $C_{x,y}$ is computed for all bands of the multispectral image of a palm. An example procedure for a single band of a palm from the PolyU database is shown in Fig. 3.

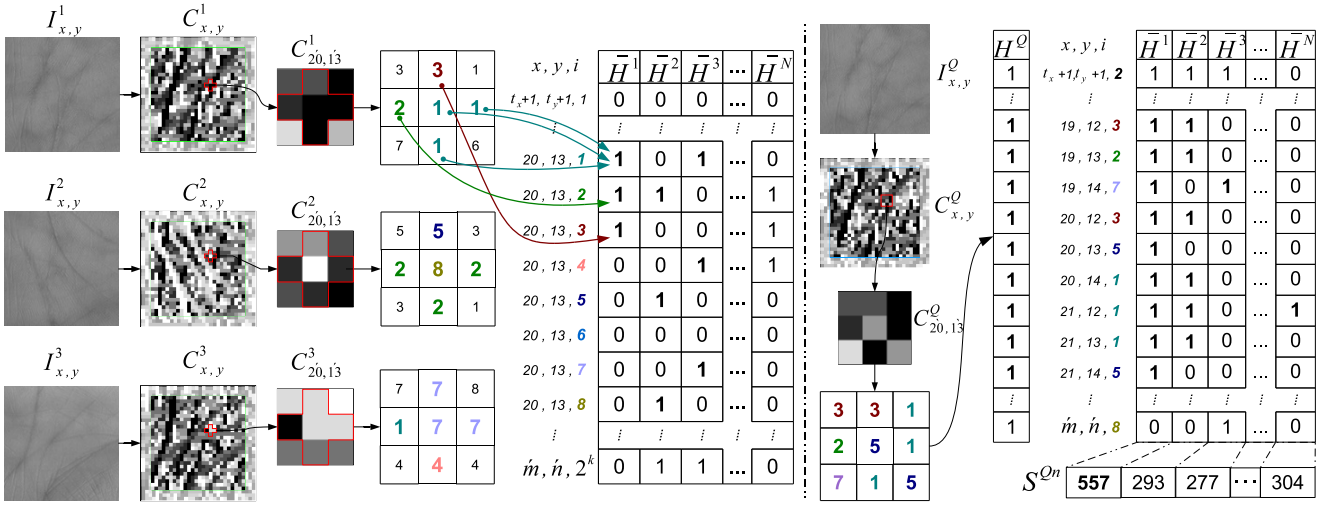

(a) (b)

Figure 4. (a) Example of binary *Contour Code* encoding. (b) Binary *Contour Code* matching. $I^{Q}_{x,y}$ is best matched to $I^{1}_{x,y}$ as H^{1} has more 1s in the hash table indexed with H^{Q} resulting in S^{Q_1} as the maximum sum (the subscript (xyi) of H is dropped for conciseness)

4.2. Binary Hash Table Encoding

Although, a code in 2^k orientations can be encoded in a minimum of k bits, in this framework, we binarize the *Contour Code* representation using 2^k bits to take advantage of a fast binary code matching. Unlike other methods which use the angular distance [16] or the hamming distance [18], we propose an efficient binary hash table based *Contour Code* matching. In a hash table, each column refers to a palm's binary hash vector derived from its *Contour Code* representation. Within a column, each hash location (x, y) has 2^k bins. We define a hash function which assigns an orientation at (x, y) to the i^{th} bin as

$$H_{(xyi)} = \begin{cases} 1, & i = C_{x,y} \\ 0, & otherwise \end{cases} \tag{2}$$

where $H_{(xyi)}$ is the binarized form[1] of a *Contour Code* representation.

Since palmprint features are deformable, it is not possible to achieve a perfect correspondence between all the features of two palm images taken at different instances of time. Therefore, it is intuitive to assign multiple orientations to the bins of a hash location based on its neighborhood. The hash function is blurred so that it assigns to each hash bin in $\bar{H}_{(xyi)}$ with the orientations in (x, y) and its neighbors.

$$\bar{H}_{(xyi)} = \begin{cases} 1, & \forall\ i = C_{\acute{x},\acute{y}} \\ 0, & otherwise \end{cases} \tag{3}$$

where $\acute{x}, \acute{y}$ is the set of (x, y) and its *4-connected* neighbors, $\{(x, y), (x \pm 1, y), (x, y \pm 1)\}$. Since, blurring depends on a neighborhood compared to a single pixel like the BOCV, it robustly captures crossover line orientations without the need of any threshold from training images. An example of *Contour Code* binarization using the blurred hash function is given in Fig. 4a.

[1] (xyi) represents a single subscript that takes on a distinct value for each combination of an element from the index sets x, y and i.

4.3. Matching

In the identification step (one-to-many matching), the query image $I^{Q}_{x,y}$ is first converted to the binary form $H^{Q}_{(xyi)}$ using equation (2). No blurring is required now, since it has already been implemented offline on all the gallery images. The match score (S^{Qn}) between $H^{Q}_{(xyi)}$ and $\bar{H}^{n}_{(xyi)}$, $n = 1, 2, 3..., N$ is computed as

$$S^{Qn} = \|\bar{H}^{n}_{(xyi)} \quad \forall \quad \arg\limits_{(xyi)} H^{Q}_{(xyi)} = 1\|_0 \tag{4}$$

where $\|.\|_0$ is the L_0-norm which is the number of non-zero elements in $\bar{H}^{n}_{(xyi)}$ for all (xyi) indices where $H^{Q}_{(xyi)}$ is 1. The hash table, after indexing, produces a relatively sparse binary array whose summation is more efficient. Since, the L_0-norm of a binary vector is equivalent to the summation of all the vector elements, equation (4) can be synonymously written as

$$S^{Qn} = \sum\{\bar{H}^{n}_{(xyi)} \quad \forall \quad \arg\limits_{(xyi)} H^{Q}_{(xyi)} = 1\} \tag{5}$$

The matching procedure is illustrated in Fig. 4b.

Apart from the blurring, which caters for minor orientation location errors within an ROI, during matching, the query image is shifted $\pm t_x$ pixels horizontally and $\pm t_y$ pixels vertically to cater for the misalignment between different ROIs. Consequently, the overlapping region of the two images to match reduces to $(\acute{m}{=}m - 2t_x, \acute{n}{=}n - 2t_y)$ pixels.

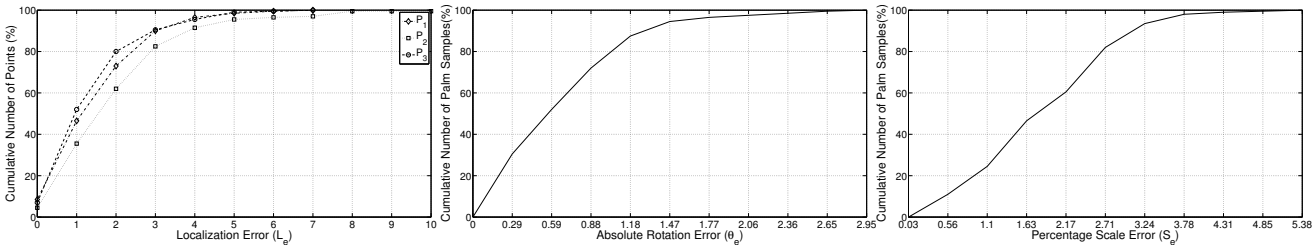

(a) (b) (c)

Figure 5. ROI extraction error evaluation. (a) Cumulative percentage of points detected within a *Localization Error* (L_e). (b) Cumulative percentage of palm samples within an *Absolute Rotation Error* (θ_e). (c) Cumulative percentage of palm samples within a *Scale Error* (S_e)

Therefore, only the central $\acute{m} \times \acute{n}$ region of a *Contour Code* representation is required to be stored in a hash table. The final class is determined by the maximum score among all the translated matches.

$$Class = \arg\max_{n}(S^{Qn}_{t_x,t_y}) \tag{6}$$

We selected $t_x, t_y = 3$, since no improvement in match score was observed for translation beyond ± 3 pixels. The indexing is independent of the size of the database and is only dependent on the valid ROI size being matched $(\acute{m} \times \acute{n})$. In our implementation, we vertically stacked the hash tables of all the bands to compute the aggregate match score in a single step. As the match score is an integer, no floating point comparisons are required for the final class decision.

In case of verification (1-1 matching), the query palm may be matched with the palm samples of the claimed identity only. Thus the effective width of the hash table will be equal to the number of palm samples of the claimed identity but its height will remain the same$(2^k \acute{m}\acute{n})$.

5. Experimental Results

5.1. ROI extraction accuracy

The ability of accurately localizing the landmarks was determined by comparison with a subjective selection of landmarks for 200 multispectral images in the CASIA database (manual selections were averaged over the six bands). We define the localization error as the Chebyshev distance between the manually selected and the automatically extracted landmarks. The localization error (L_e), between two landmarks can be computed as

$$L_e = \max(|x_m - x_a|, |y_m - y_a|) \tag{7}$$

where (x_m, y_m), (x_a, y_a) correspond to the manually and automatically identified landmarks respectively. The localization error is 1 if the located landmark falls within first 8 neighboring pixels, 2 if it falls in the first 24 neighboring pixels and so on. Similarly, the absolute rotation error (θ_e) between two palm samples is

$$\theta_e = |\theta_m - \theta_a| \tag{8}$$

where θ_m and θ_a correspond to the angle of rotation of palm computed from manual and automatic landmarks respectively. Finally, the percentage scale error (S_e) is

$$S_e = \left(\max\left(\frac{S_m}{S_a}, \frac{S_a}{S_m}\right) - 1\right) \times 100\% \tag{9}$$

where S_m is the manually identified palm width averaged over three measurements; S_a is automatically calculated.

Fig. 5a shows the localization error between the manually selected and the automatically extracted landmarks. It can be observed that the three landmarks were located in an $L_e \leq 4$ for more than 90% of the samples. All the ROIs were extracted in a $\theta_e \leq 2.95^\circ$ (Fig. 5b). The ROI extraction is robust to rotational variations given the overall absolute rotational variation, $(\mu_\theta, \sigma_\theta) = (20.7^\circ, 7.24^\circ)$ of the CASIA database. Finally, all ROIs were extracted in $S_e \leq 5.4\%$ (Fig. 5c). A few sample images with different rotation, scale and translation variation and the extracted ROIs are shown in Fig. 6. Note that despite the variations, the ROIs are reliably extracted.

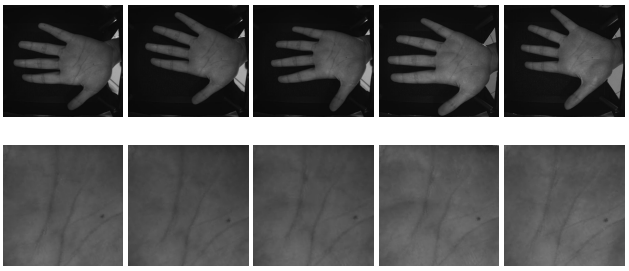

Figure 6. Extracted ROIs for a variety of hand movements between different samples of a person.

5.2. Pyramidal-Directional Filter Pair Selection

The selection of appropriate pyramidal/directional filter is critical to robust feature extraction. It is important to emphasize that the ability of a filter to capture robust line like features in a palm indirectly relates to the final recognition accuracy. Hence, we can regard the pyramidal/directional filter combination with the lowest recognition error rate as the best. For evaluating the verification performance of the proposed *Contour Code*, a query palm is matched with all

other palms in the database. A match is genuine if the matched palm sample belongs to the same subject as the query palm, otherwise it is declared as imposter. The *Receiver Operating Characteristics (ROC)* curve, which depicts the variation of *False Accept Rate (FAR)* with the *False Reject Rate (FRR)* is computed for the recognition experiments. The *Equal Error Rate (EER)* which is the value at which the *FAR* equals the *FRR*, is selected as the evaluation criterion.

We tested all possible pairs of 4 pyramidal and 10 directional filters available in the Nonsubsampled Contourlet Toolbox [26]. As shown in Table 2, the *pyrexc* filter consistently achieves lower *EER* compared to the other three pyramidal decomposition filters for all combinations of the directional filters. Moreover, the *sinc* filter exhibits lowest *EER* which shows its best directional feature capturing characteristics. It should be noted that the *pkva* filter is a better choice for directional filter when using the *9-7*, *maxflat* or *pyr* filter at the pyramidal decomposition stage which also explains a mutually dependent relationship between pyramidal and directional filters. Based on the results, we select the *pyrexc-sinc* filter combination for *Contour Code* representation in all experiments.

D_f \ P_f	**9-7**	**maxflat**	**pyr**	**pyrexc**
cd	0.0182	0.0255	0.0175	0.0182
dvmlp	0.0480	0.0485	0.0303	0.0311
haar	0.0727	0.0764	0.0424	0.0394
ko	0.0727	0.0764	0.0515	0.0475
kos	0.0777	0.0764	0.0424	0.0436
lax	0.0777	0.0368	0.0156	0.0125
pkva	**0.0121**	**0.0121**	**0.0084**	0.0077
sinc	0.0133	0.0152	0.0091	**0.0061**
sk	0.0182	0.0273	0.0182	0.0175
vk	0.0345	0.0388	0.0214	0.0160

Table 2. *EER* for combinations of pyramidal and directional filters in *Contour Code* on the PolyU multispectral palmprint database

5.3. Recognition Results on the PolyU database

For the PolyU database, 6000x$5999/2$=$17,997,000$ matches are computed in total. The number of genuine scores is 12x11x$500/2$=$33,000$ and the remaining $17,964,000$ are imposter scores.

Firstly, we test the individual capability of the bands for recognition. Among the four bands of PolyU database, the 660nm band performs the best (*EER=0.0242%*) followed by 525nm (*0.0420%*), 470nm (*0.0784%*) and 880nm (*0.1030%*). This shows the presence of more discriminatory features in the 660nm band compared to the rest of the bands since it partially captures both line and vein features.

For the score level fusion of bands, the *Contour Code* achieves a lowest *EER* of 0.0061%. A comparison of *EER* with the other methods is given in Table 3. The comparison shows the superiority of the proposed *Contour Code* which achieves at least 50% reduction in *EER* compared to the state-of-the-art CompCode and other methods. A 100% identification rate was also be achieved by treating the first sample of each palm as gallery and the rest as probes.

Method (PolyU database)	**EER (%)**
CompCode with Wavelet Fusion [8]	0.0696
Joint Palmprint and Palmvein [11]	0.0158
CompCode with Score-Level Fusion [1]	0.0121
Contour Code	**0.0061**
Method (CASIA database)	**EER (%)**
Curvelet Fusion with OLOF [18]	0.50[2]
Wavelet Fusion with ACO [19]	3.125
Contour Code	**0.300**

Table 3. Comparison of the *Contour Code* with other methods on the PolyU and CASIA multispectral palmprint databases.

5.4. Recognition Results on the CASIA database

A similar experimental setup is selected for the evaluation of *Contour Code* on the CASIA database. There are $719,400$ matches in total out of which only 3000 are genuine and the rest are imposter. For the six individual bands of CASIA database the performance of bands arranged in increasing EER was (White (*0.615%*), 850nm (*0.758%*), 940nm (*0.778%*), 630nm (*0.799%*), 460nm (*0.828%*), 700nm (*1.559%*)).

A score level band fusion achieves an EER of 0.300%. A comparison with other methods is given in Table 3. The *Contour Code* outperforms the state-of-the-art OLOF by achieving a 40% reduction in the *EER*. The *EER* of *Contour Code* on CASIA database is higher relative to the PolyU database because of the higher variation in translation, scale and rotation. A 99.7% identification rate was achieved using a single sample in gallery and the rest as probes.

5.5. Discussion

We evaluate the statistical significance of the improvement in EERs using the method described by Guyon *et al*. [27]. For n trials, (genuine + imposter matches) the smallest error rate (p) that guarantees statistical significance with a confidence of $(1-\alpha)$, within a pessimistic bound $|p-\hat{p}| \leq \beta p$, (where $\hat{p}$ is the empirical test error rate) is

$$p = \frac{-2\ln\alpha}{\beta^2 n} \tag{10}$$

In case of PolyU database, the statistical significance can be guaranteed for an *EER* above 0.0013% with a high confidence of 99% ($\alpha = 0.01$) and $\beta = 0.2$. For the CASIA database, the statistical significance of the EER can be guaranteed above 0.0320%. The EERs achieved by the *Contour Code* are safely above these limits and still lower than the other methods by at least 40%.

[2]This result was reported on a database of 330 hands. However, only a subset of the database comprising 200 hands has been made public

The computational complexity of matching is critical in practical identification scenarios because databases can be quite large. The binary Contour Code matching has been designed to carry out operations that are of low computational complexity. It comprises an indexing part whose complexity is independent of the database size and results in a relatively sparse binary matrix. Summing a column of this matrix corresponds to score level fusion of the multispectral bands of an individual. A MATLAB implementation on a 2.67 GHz machine with 8 GB RAM can perform over $70,000$ matches per second per band. The *Contour Code* extraction takes only 43ms per band and requires only 676 bytes per band for storage.

6. Conclusion

We presented *Contour Code*, a novel multidirectional representation and binary hash table encoding for robust and efficient multispectral palmprint recognition. An automatic technique was designed for the extraction of a region of interest from palm images acquired with noncontact sensors. Unlike existing methods, we report quantitative results of ROI extraction by comparison with ground truth. The *Contour Code* exhibits robust multispectral feature capturing capability and outperformed existing state-of-the-art techniques on two standard databases *i.e*. PolyU and CASIA. Binary encoding of the *Contour Code* in a hash table facilitates simultaneous matching to the database and score level fusion of the multispectral bands in a single step. Unlike existing techniques, normalization of scores is not required before fusion. The *Contour Code* is a generic orientation code for line-like features and can be extended to other biometric traits including fingerprints and fingerknuckle prints.

Acknowledgment

This research was supported by ARC Grant DP0881813 and DP110102399. The first author was an IPRS scholar in Australia. Authors acknowledge the Polytechnic University of Hong Kong for providing the PolyU-MS-Palmprint database and the Chinese Academy of Sciences' Institute of Automation for providing the CASIA-MS-PalmprintV1 database.

References

[1] D. Zhang, Z. Guo, G. Lu, L. Zhang, and W. Zuo, "An online system of multispectral palmprint verification," *IEEE Transactions on Instrumentation and Measurement*, vol. 59, no. 2, pp. 480–490, 2010.

[2] Z. Pan, G. Healey, M. Prasad, and B. Tromberg, "Face recognition in hyperspectral images," *IEEE Transactions on Pattern Analysis and Machine Intelligence*, vol. 25, no. 12, pp. 1552–1560, 2003.

[3] W. Di, L. Zhang, D. Zhang, and Q. Pan, "Studies on hyperspectral face recognition in visible spectrum with feature band selection," *IEEE Trans. SMC, Part A*, vol. 40, no. 6, pp. 1354–1361, 2010.

[4] C. Boyce, A. Ross, M. Monaco, L. Hornak, and X. Li, "Multispectral iris analysis: A preliminary study," in *CVPR Workshop*, 2006.

[5] R. Rowe, U. Uludag, M. Demirkus, S. Parthasaradhi, and A. Jain, "A multispectral whole-hand biometric authentication system," in *IEEE Biometrics Symposium*, 2007, pp. 1–6.

[6] A. Jain, A. Ross, and S. Prabhakar, "An introduction to biometric recognition," *IEEE Transactions on Circuits and Systems for Video Technology*, vol. 14, no. 1, pp. 4–20, 2004.

[7] Y. Hao, Z. Sun, and T. Tan, "Comparative studies on multispectral palm image fusion for biometrics," in *ACCV*, 2007, pp. 12–21.

[8] D. Han, Z. Guo, and D. Zhang, "Multispectral palmprint recognition using wavelet-based image fusion," in *ICSP*, 2008, pp. 2074–2077.

[9] A. Kong, D. Zhang, and M. Kamel, "A survey of palmprint recognition," *Pattern Recognition*, vol. 42, no. 7, pp. 1408–1418, 2009.

[10] D.-S. Huang, W. Jia, and D. Zhang, "Palmprint verification based on principal lines," *Pattern Recog.*, vol. 41, no. 4, pp. 1316–1328, 2008.

[11] D. Zhang, Z. Guo, G. Lu, L. Zhang, Y. Liu, and W. Zuo, "Online joint palmprint and palmvein verification," *Expert Systems with Applications*, vol. 38, no. 3, pp. 2621–2631, 2011.

[12] J. Wang, W. Yau, A. Suwandy, and E. Sung, "Fusion of palmprint and palm vein images for person recognition based on laplacianpalm feature," in *CVPR*, 2007, pp. 1–8.

[13] G. Lu, D. Zhang, and K. Wang, "Palmprint recognition using eigenpalms features," *Pattern Recognition Letters*, vol. 24, no. 9-10, pp. 1463–1467, 2003.

[14] X. Wu, D. Zhang, and K. Wang, "Fisherpalms based palmprint recognition," *Patt. Recog. Lett.*, vol. 24, no. 15, pp. 2829–2838, 2003.

[15] X. Xu and Z. Guo, "Multispectral palmprint recognition using quaternion principal component analysis," *IEEE Workshop on Emerging Techniques and Challenges for Hand-Based Biometrics*, pp. 1–5, 2010.

[16] A. Kong and D. Zhang, "Competitive coding scheme for palmprint verification," in *ICPR*, 2004, pp. 520–523.

[17] Z. Sun, T. Tan, Y. Wang, and S. Z. Li, "Ordinal palmprint represention for personal identification," in *CVPR*, 2005, pp. 279–284.

[18] Y. Hao, Z. Sun, T. Tan, and C. Ren, "Multispectral palm image fusion for accurate contact-free palmprint recognition," in *Proc. ICIP*, 2008, pp. 281–284.

[19] D. Kisku, P. Gupta, J. Sing, and C. Hwang, "Multispectral palm image fusion for person authentication using ant colony optimization," in *IEEE Workshop on Emerging Techniques and Challenges for Hand-Based Biometrics*, 2010, pp. 1–7.

[20] Z. Guo, D. Zhang, L. Zhang, and W. Zuo, "Palmprint verification using binary orientation co-occurrence vector," *Pattern Recognition Letters*, vol. 30, no. 13, pp. 1219–1227, 2009.

[21] PolyU Multispectral Palmprint Database. [Online]. Available: http://www.comp.polyu.edu.hk/~biometrics/MultispectralPalmprint/MSP.htm

[22] CASIA Multispectral Palmprint Database. [Online]. Available: http://www.cbsr.ia.ac.cn/MS_Palmprint_Database.asp

[23] D. Zhang, W. Kong, J. You, and M. Wong, "Online palmprint identification," *IEEE TPAMI*, vol. 25, no. 9, pp. 1041–1050, 2003.

[24] A. L. da Cunha, J. Zhou, and M. N. Do, "The nonsubsampled contourlet transform: Theory design and applications," *IEEE Transactions on Image Processing*, vol. 15, no. 10, pp. 3089–3101, 2006.

[25] M. N. Do and M. Vetterli, "The contourlet transform: an efficient directional multiresolution image representation," *IEEE Transactions on Image Processing*, vol. 14, no. 12, pp. 2091–2106, 2005.

[26] A. Cunha. The Nonsubsapled Contourlet Toolbox. [Online]. Available: http://www.mathworks.com/matlabcentral/fileexchange/10049

[27] I. Guyon, J. Makhoul, R. Schwartz, and V. Vapnik, "What size test set gives good error rate estimates?" *IEEE Transactions on Pattern Analysis and Machine Intelligence*, vol. 20, no. 1, pp. 52–64, 1998.